

Channel Characterization for Wideband 60 GHz Wireless Link Within a Metal Enclosure

Seyran Khademi¹, Sundeep Prabhakar Chepuri,¹ Zoubir Irahhauten², Gerard J. M. Janssen¹ Alle-Jan van der Veen¹

¹Faculty of Electrical Engineering, Mathematics and Computer Science, Delft University of Technology, The Netherlands

²Mobile Innovation Radio group, KPN, The Netherlands

Emails: {s.khademi, s.p.chepuri,g.j.m.janssen,a.j.vanderveen}@tudelft.nl, zoubir.irahhauten@kpn.com

Abstract—A metal cabinet is chosen to emulate the environment within mechatronic systems, which have metal enclosures in general. There is no channel characterization study for such an environment to the best of our knowledge. The wireless channel impulse response has been measured in different volumes in closed metal cabinet at 60 GHz, using a frequency sounding technique for a line-of-sight (LOS) scenarios. Large root-mean-square (rms) delay spread (RDS) and very small path loss coefficients are among the distinguishing features of the developed channel model.

I. INTRODUCTION

In this paper, we investigate the channel behavior inside a metal enclosure to design a high-rate short-range wireless link for mechatronic systems at the 60 GHz license-free band. Application areas include communication within automobiles, satellites, aircrafts or industrial machineries. Usually the high data rate wireless link (peak data rate up to a few tens of Gbps) is required to transfer the information collected by several sensors to a control unit and actuators. These environments with metal enclosures are highly reflective, and the resulting “long” wireless channels make wireless communications very challenging.

Frequency domain channel sounding technique is used to acquire the channel frequency response (CFR) in our measurement campaign. The CFRs are collected for different distances of Tx and Rx antennas to obtain enough statistics for further parametric channel modeling. All measurements are done under the line-of-sight (LOS) condition when no object hinders the direct path between the transmitter and receiver. Two different volumes of the metal cabinet are examined and the results indicate a larger root-mean-square (rms) delay spread (RDS) for the bigger volume.

Even though the spectrum scarcity argument does not directly motivate the use of 60 GHz for mechatronic systems within closed metal enclosures, in which transmissions do not interfere with other existing communication systems, several properties do make communication at this free bandwidth range interesting [1].

This work is a part of the manuscript which is submitted to IEEE transactions on wireless communications, and was supported by STW under the FASTCOM project (10551).

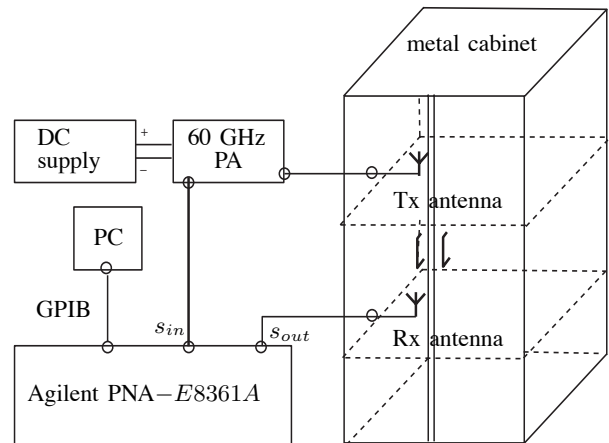


Fig. 1: Measurement setup for channel sounding inside the metal cabinet.

Small antenna size: at higher frequencies, smaller antennas, can be squeezed in a small area, and perhaps even be integrated on a chip [2]. Thus, metal enclosures with a very rich scattering environment combined with 60 GHz technology and very-large MIMO technique [3] could enable high data rates comparable to wired systems.

Physical available bandwidth: More physical bandwidth is available when we go to higher carrier frequencies. E.g., the physical bandwidth that can be used at $f_c = 2.4$ GHz is limited compared to 7 GHz free spectrum at 60 GHz.

II. MEASUREMENT SET-UP

The set-up depicted in Fig. 1 is used to measure the channel impulse response (CIR) inside a metal cabinet. The procedure is as follows.

First, the channel frequency response (CFR) is measured using a PNA-E series microwave vector network analyzer (VNA) E8361A from Agilent. Due to the losses inside the VNA and 60 GHz co-axial cables, the measured signal at the receiver is weak. A 60 GHz solid state power amplifier (PA) from QuinStar Inc. (QGW-50662030-P1) was used to compensate for the losses and to improve the dynamic range.

As transmit and receive antennas, we used two identical open waveguide antennas operating at 50-75 GHz frequency

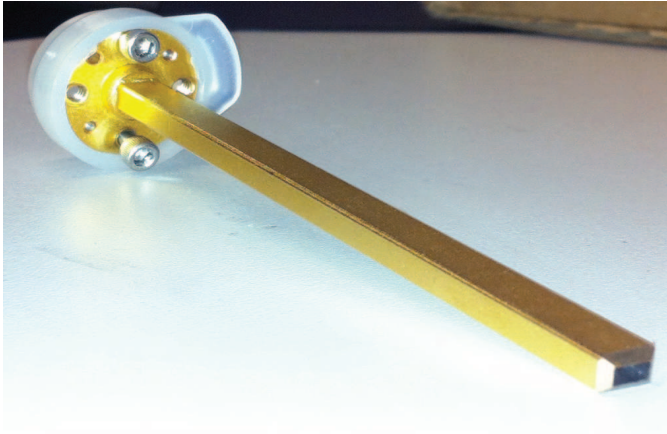


Fig. 2: Open waveguide antennas for the 50-75 GHz frequency band, with aperture size $3.759 \times 1.880 \text{ mm}^2$.

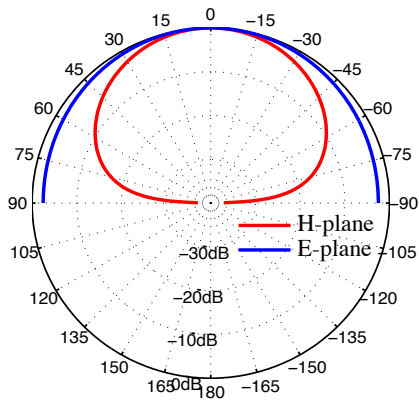


Fig. 3: Field radiated by the TE_{10} mode in open waveguide antenna with respect to θ angle.

band, with aperture size $3.759 \times 1.880 \text{ mm}^2$, which is shown in Fig. 2. Radiation pattern for the used open waveguide antenna is simulated in Matlab, as depicted in Fig. 3. The radiated pattern at half E-plane is nearly isotropic.

The measurement bandwidth is set to $B_w = 5 \text{ GHz}$, and the channel is sampled from 57 GHz to 62 GHz at $N_s = 12001$ frequency points. This results in a frequency spacing of $\Delta f_s = 0.416 \text{ MHz}$, so that the time resolution is $\tau_{res} = \frac{1}{B_w} = 0.2 \text{ ns}$ and the maximum measurable excess delay is $\tau_{max} = 2400 \text{ ns}$.

To investigate the channel behavior within the metal cabinet, we considered two LOS scenarios. *Scenario 1* where we used a metal enclosure of dimension $100 \times 45 \times 45 \text{ cm}^3$ and *Scenario 2* where a metal enclosure of a larger dimension is examined, i.e., $100 \times 45 \times 180 \text{ cm}^3$.

For both scenarios, the location of the transmit antenna was kept fixed. The channel was measured at various locations in 3 dimensions, i.e., x, y, z axes, as specified in Table I. This produced 96 receiver locations for both the considered

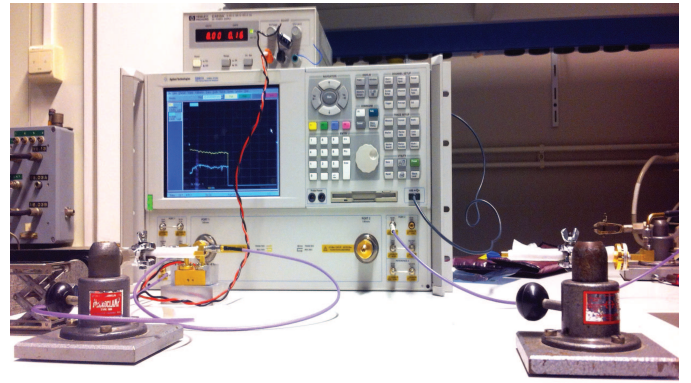


Fig. 4: Reference LOS measurement for calibration and excluding the antenna effects on the CIR. Two waveguide antennas are covered with soft tissues (for protection) and placed at a distance of 25 cm with an aid of two stand holders to avoid possible movements during the measurement.

scenarios. The transmit antenna was fixed at co-ordinate

	x -axis	y -axis	z -axis
Scenario 1	15-85 cm; 8 steps	5-30 cm; 6 steps	15, 30 cm
Scenario 2	15-85 cm; 8 steps	5-30 cm; 6 steps	35, 140 cm

TABLE I: Receive antenna co-ordinates.

$(x_t, y_t, z_t) = (65, 15, 0) \text{ cm}$ for all measurements.

III. DATA PROCESSING

Post-processing of the data is required to extract the CIR from the measured frequency domain signals. Prior to the IFFT, we compensate the antenna and instrument responses using an inverse filtering technique [4], [5]. This method uses a reference LOS measurement by placing the transmitter and receiver at a distance of 25 cm outside the metal cabinet (free space). The setting for reference LOS measurement is shown in Fig. 4. The CFR for each measurement is obtained by excluding the CFR of the reference measurement, as it represents (approximately) the combined impulse response of the transmit and receive antennas and the measurement system. For more detailed explanation see [1].

A sample CIR after and before inverse filtering is shown in Fig. 5. It is clear that the channel is still well above the noise level even after 1000 ns. It should be noted, that the delay introduced by the cables and system are removed from the calibrated CIR after inverse filtering.

We performed power normalization for model parameters, that do not depend on the absolute power (i.e., the small-scale channel model). The dynamic range of the received signal is in the order of 70 dB, considering the noise level at -70 dB after normalization to zero dB. To reduce the computational complexity and also to avoid windowing artifact after inverse discrete Fourier transform (IDFT), the tail of the channel impulse response is truncated for further parameter estimations. We apply a threshold level taking into account

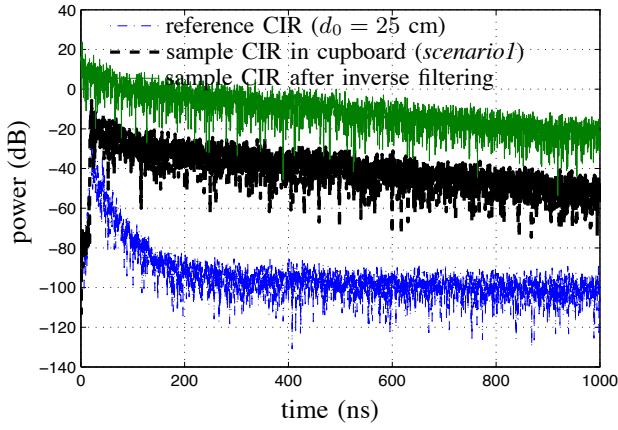


Fig. 5: Sample CIR from *scenario 1* before and after inverse filtering with Tx-Rx $d = 33$ cm apart, compared to the measured reference CIR (free space, Tx-Rx $d_0 = 25$ cm apart).

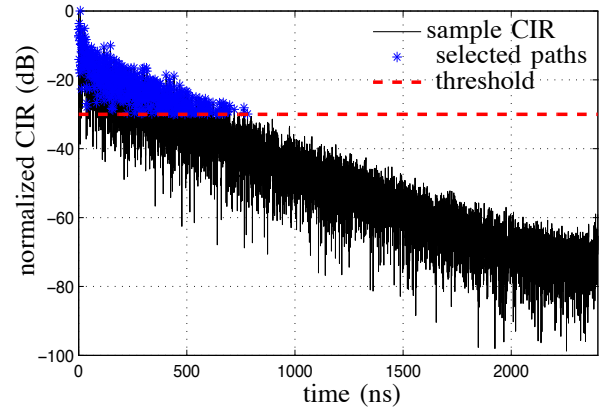


Fig. 7: Sample CIR with 30 dB threshold and received paths for *scenario 1*.

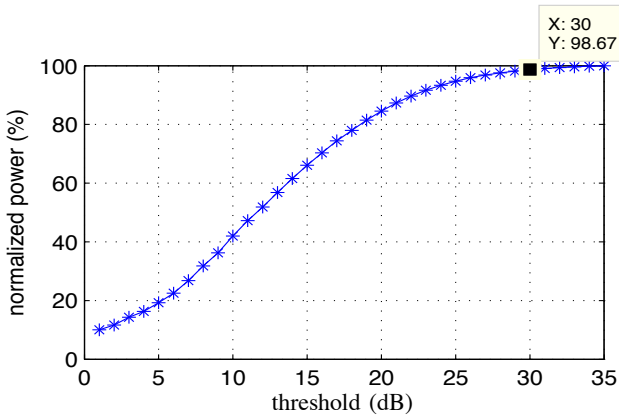


Fig. 6: Average received power for different thresholds in *scenario 1*.

the noise level, the amount of total received power and the relevant multipath components [6], [7].

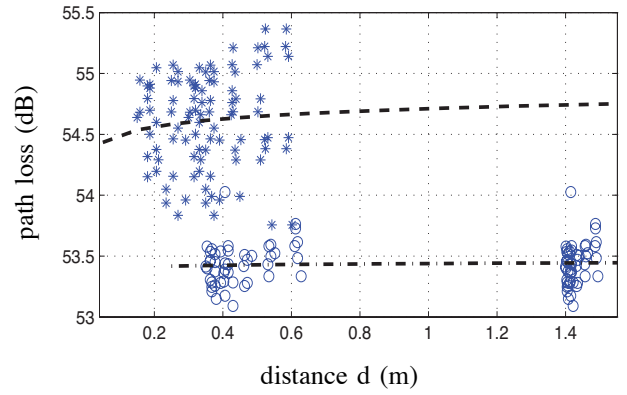
As can be seen in Fig. 6, 98% of the total power is captured by fixing the threshold on 30 dB which is almost 40 dB above the noise level. In Fig. 7, interestingly, the remaining CIR is about 800 ns which is very unusual compared to typical indoor channels reported in the literature.

IV. LARGE-SCALE CHANNEL MODEL: PATH-LOSS

The large-scale channel model parameterizes the transmission loss as well as fading due to blockage and shadowing, statistically. It is essential for any wireless system to study the large scale behavior of the channel for further link budget calculation and modeling the channel variation aspects. The path-loss model can be written in logarithmic scale as

$$P_L(d)_{dB} = P_L(d_0)_{dB} + \alpha 10 \log_{10}\left(\frac{d}{d_0}\right) + X_\sigma, \quad (1)$$

where $P_L(d)_{dB}$ is the average received power at a distance d (m) relative to a reference distance d_0 (m), α represents the path-loss exponent, and X_σ is a log-normal random variable

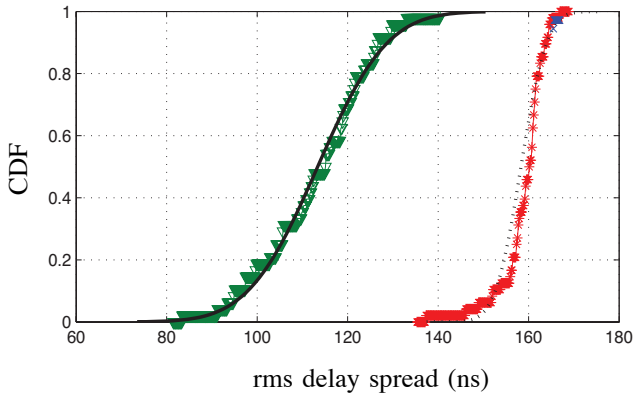


- * measured data *scenario 1*
- $P_L(d) = 54.711 + 0.021 \cdot 10 \log_{10}(d)$
- measured data *scenario 2*
- .- $P_L(d) = 53.439 + 0.004 \cdot 10 \log_{10}(d)$

Fig. 8: Path-loss as function of distance.

with standard deviation σ [dB] reflecting the variation (in dB) caused by flat fading (shadowing or slow fading). The formula (1) suggests that the average received power decreases exponentially with increasing distance between transmitter and receiver.

The path-loss exponent α is obtained by measuring the received power for different distances between the transmit and receive antennas. The distance related path loss term ($P_t - P_r$) in Fig. 8 shows that the path-loss exponent α is very small (around 0.02-0.004), suggesting that in such a closed metal environment there is nearly no loss in the received power as function of distance. When compared to narrowband indoor systems some measurements have reported a path-loss exponent of α in the range 1.6 – 6 [4].



—▽— measured data *scenario1*
 — normal fitting: $(\mu, \sigma)=(113.4, 12.1)$
 —*— measured data *scenario2*
 normal fitting: $(\mu, \sigma)=(159.1, 5.1)$

Fig. 9: Cumulative distribution function of RDS.

V. SMALL-SCALE CHANNEL MODEL: RMS DELAY SPREAD (RDS)

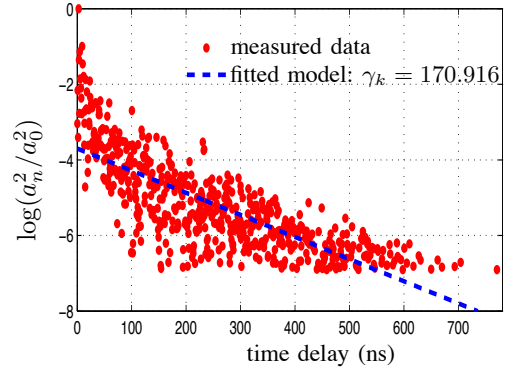
A wireless channel can be characterized by its small-scale properties caused by the reflections in the environment, which are modeled as multipath components. Some of the important parameters that describe the small-scale variations are the RDS, and the time decay constant (TDC).

A. RMS delay spread

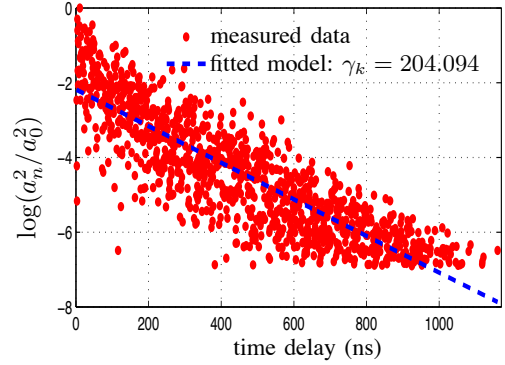
The RMS delay spread describes the time dispersion of the channel, i.e., the distribution of the received power in time. A large delay spread causes severe inter-symbol interference (ISI) and can deteriorate the system performance. The RDS is obtained by first estimating the individual path parameters $\{(a_n^2, t_n)\}$ for each observation, and then computing

$$t_{rms} = \sqrt{\bar{t}^2 - (\bar{t})^2}, \quad \bar{t}^\beta = \frac{\sum_{n=1}^N a_n^2 t_n^\beta}{\sum_{n=1}^N a_n^2},$$

where \bar{t} , \bar{t}^2 and \bar{t}^β are the first, second and β moment of the power delay profile, respectively. Fig. 9 shows the cumulative distribution function (CDF) of the estimated RDS values for both the scenarios. The mean value of the normal distribution, obtained after fitting, reveals the average length of the channel. We obtained values of 113.4 ns (*scenario 1*), and 159.1 ns (*scenario 2*). These mean RDS values are significantly larger than that of the conventional indoor channels, which are typically in the range 4 – 21 ns. The larger RDS values will impact the signal processing and system design, e.g., the channel equalization and residual inter block interference (IBI) after equalization, and hence, the achievable data rates.



(a) sample measurement in *Scenario 1*



(b) sample measurement in *Scenario 2*

Fig. 10: LS fit for time decay constant is leading to an estimated γ_k (ns) for each measurement.

B. Time decay constant

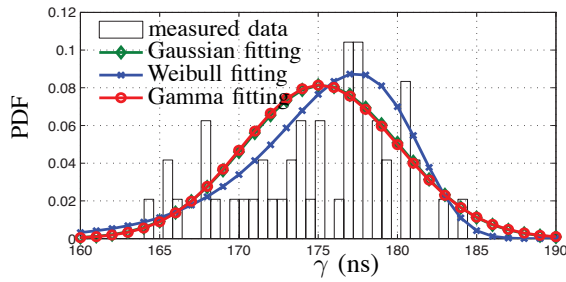
The current IEEE standard channel models are mostly based on the Saleh-Valenzuela (SV) model [8], [9]. In the SV channel model, the multipaths are considered as a number of rays arriving within different clusters, and separate power decay constants are defined for the rays and the clusters.

Our measurement results do not show that the multipath components form clusters. A physical justification comes from the fact that multipath reflections are coming from the (same) walls. In this case, the average power delay profile (PDP) is defined by only one decay parameter γ rather than the common SV model with two decay parameters. The model with one decay parameter is given by

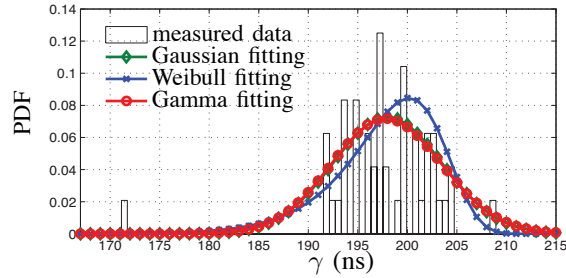
$$\bar{a}_n^2 = \bar{a}_0^2 \exp(-t_n/\gamma), \quad (2)$$

where \bar{a}_0^2 and \bar{a}_n^2 are the (statistical) average power of the first and n th multipath component, respectively, and γ is the power decay time constant for arriving rays, assumed as a random variable. We estimate γ for each measurement in every scenario using a least-squares curve fitting on $\log(a_n^2)/\log(a_0^2)$, as shown in Fig. 10.

After estimating γ_k s for all of measurements, the statistical parameter for time decay constant is characterized by the best fitted probability density function (PDF) for γ . Gaus-



(a) Scenario 1
 Gaussian(μ, σ) = (175.2, 4.901)
 Gamma(α, β) = (1281, 0.137)
 Weibull(ζ, k) = (177.5, 42.28)



(b) Scenario 2
 Gaussian(μ, σ) = (197.9, 5.481)
 Gamma(α, β) = (1265, 0.156)
 Weibull(ζ, k) = (200.3, 46.05)

Fig. 11: PDF fittings for time decay constant γ .

sian, Gamma, and Weibull distributions are commonly used to statistically model γ [5], [6]. Here we examined these three distributions for our measured data and the results are presented in Fig. 11.

For the Gaussian distribution μ and σ represent the mean and standard deviation, respectively, for the fitted PDF. For the Gamma distribution, the parameters α and β are computed for all scenarios from the empirical data. The Gamma distribution is given by

$$f(x|\alpha, \beta) = \frac{x^{\alpha-1}}{\beta^\alpha \Gamma(\alpha)} \exp(-\frac{x}{\beta}), \quad (3)$$

where $\Gamma(\alpha)$ is a Gamma function.

The scale and shape parameters are ζ and k , respectively, for the Weibull distribution which is given by

$$f(x|\zeta, k) = \begin{cases} \frac{k}{\zeta^k} x^{k-1} \exp(-(\frac{x}{\zeta})^k) & \text{if } x \geq 0 \\ 0 & \text{if } x < 0 \end{cases} \quad (4)$$

The estimated TDC parameters are significantly large compared to the typical indoor wireless channels. For instance, in IEEE 802.15 standard for the CM1, CM4 and CM9 channels, reported mean γ values (Gaussian) are in order of 4.35, 0.42 and 61.1, respectively [10]. Obviously, this indicates the non damping environment inside the metal cabinet as it reflects in other model parameters as well.

VI. CONCLUSIONS

A parametric channel model has been proposed for the 60 GHz band in an environment within a metal enclosure. The most distinguishing features compared to conventional indoor environments are the very small path-loss exponent and significantly longer channel. This behavior is caused by the non-damping effect of the metal walls, and needs for more sophisticated channel equalization schemes to combat such long channels.

REFERENCES

- [1] S. Khademi, S. P. Chepuri, Z. Irahauten, G. J. M. Janssen, and A.-J. van der Veen, "60 GHz wireless link within metal enclosures: Channel measurements and system analysis," *arXiv:1311.4439*, Nov. 2013.
- [2] K. K. O, K. Kim, B. A. Floyd, and others., "On-chip antennas in silicon ICs and their application," *IEEE Trans. Electron Devices*, vol. 52, no. 7, pp. 1312–1323, 2005.
- [3] F. Rusek, D. Persson, B. K. Lau, E. Larsson, T. Marzetta, O. Edfors, and F. Tufvesson, "Scaling up MIMO: Opportunities and challenges with very large arrays," *IEEE Signal Process. Mag.*, vol. 30, no. 1, pp. 40–60, Jan. 2013.
- [4] Z. Irahauten, *Ultra-Wideband Wireless Channel: Measurements, Analysis and Modeling*. Delft University of Technology, Dept. EEMCS, The Netherlands, 2008.
- [5] Z. Irahauten, A. Yarovoy, G. Janssen, H. Nikoogar, and L. Ligthart, "Ultra-wideband indoor propagation channel: Measurements, analysis and modeling," in *Proc. of EuCAP*, Nov. 2006, pp. 1–6.
- [6] Z. Irahauten, H. Nikoogar, and G. J. M. Janssen, "An overview of ultra wide band indoor channel measurements and modeling," *IEEE Microw. Wireless Compon. Lett.*, vol. 14, no. 8, pp. 386–388, Aug. 2004.
- [7] Z. Irahauten, A. Yarovoy, G. J. M. Janssen, H. Nikoogar, and L. Ligthart, "Suppression of noise and narrowband interference in uwb indoor channel measurements," in *Proc. of ICU*, 2005, pp. 108–112.
- [8] A. Saleh and R. Valenzuela, "A statistical model for indoor multipath propagation," *IEEE J. Sel. Areas Commun.*, vol. 5, no. 2, pp. 128–137, Jan. 1987.
- [9] Q. Spencer, M. Rice, B. Jeffs, and M. Jensen, "A statistical model for angle of arrival in indoor multipath propagation," in *Proc. of VTC*, vol. 3, 1997, pp. 1415–1419.
- [10] "IEEE standard for high rate wireless personal area networks (WPANs): Millimeter-wave-based alternative physical layer extension," *IEEE Std 802.15.3c-2009 (Amendment to IEEE Std 802.15.3-2003)*, pp. c1–187, Dec. 2009.